An atlas of bright star spectra in the near infrared from *Cassini*-VIMS

Paul N. Stewart and Peter G. Tuthill

Sydney Institute for Astronomy

School of Physics, The University of Sydney, NSW 2006, Australia

p.stewart@physics.usyd.edu.au

Philip D. Nicholson

Department of Astronomy

Cornell University, Ithaca, NY 14853, USA

G. C. Sloan

Cornell Center for Astrophyics and Planetary Science

Cornell University, Ithaca, NY 14853, USA

Carl Sagan Institute

Cornell University, Ithaca, NY 14853, USA

and

Matthew M. Hedman

Department of Physics

University of Idaho, Moscow, ID 83844, USA

Received _____; accepted _____

ABSTRACT

We present the *Cassini* Atlas Of Stellar Spectra (CAOSS), comprised of near-infrared low-resolution spectra of bright stars recovered from space-based observations by the *Cassini* spacecraft. The 65 stellar targets in the atlas are predominately M, K and S giants. However it also contains spectra of other bright nearby stars including carbon stars and main sequence stars from A to F. The spectra presented are free of all spectral contamination caused by the Earth's atmosphere, including the detrimental telluric molecular bands which put parts of the near-infrared spectrum out of reach of terrestrial observations. With a single instrument, a spectro-photometric dataset is recovered that spans the near-infrared from 0.8 to 5.1 microns with spectral resolution ranging from R=53.5 to R=325. Spectra have been calibrated into absolute flux units after careful characterisation of the instrumental spectral efficiency. Spectral energy distributions for most stars match closely with literature values. All final data products have been made available online.

1. Introduction

The recovery of high quality stellar spectra underpins an integral part of our understanding of stellar composition, evolution, and temporal behaviour. Unfortunately important molecular spectral features expected to be present are masked by the existence of the same molecular species in our own atmosphere. This is especially true for cooler evolved stars, where substantial quantities of H_2O and CO_2 are known to form. This results in large parts of the infrared region being effectively opaque to ground-based observations. Piercing this veil is only possible by observing beyond the Earth's atmosphere from space-based

platforms.

There has yet to be a space-based spectrometer dedicated to surveying bright stars over a broad range of infrared wavelengths, despite the potential scientific merit and the severe obstacles to observing from the ground. However, the Visual and Infrared Mapping Spectrometer (VIMS) instrument on the *Cassini* spacecraft has measured the spectra of many bright stars in the wavelength range of 0.8-5.1 microns. This broad wavelength range is distinct from any other existing space-based observatory platform. The International Ultraviolet Explorer (IUE) provides a survey of spectra shorter than this range, spanning 0.11 to 0.32 μm (Boggess et al. 1978). The longer wavelengths overlap with surveys by the Short Wave Spectrometer (SWS) on ESA's Infrared Space Observatory (ISO) covering 2.38 to 45.2 μm (de Graauw et al. 1996). The Space Telescope Imaging Spectrograph (STIS) on the Hubble Space Telescope (HST) can observe spectra between 0.11 and 1.0 μm (Woodgate et al. 1998), while the Near Infrared Camera and Multi-Object Spectrometer (NICMOS) on HST was capable of observing the remaining 1.0 - 2.5 μm range at the shorter end of the infrared (Thompson et al. 1998). However, these HST instruments have not been used for survey purposes and therefore only specifically targeted objects have been observed. Photometry in the *H*, *K*, *L*, and *M* bands was acquired for 92 of the brightest stars by the Diffuse Infrared Background Experiment (DIRBE) on COBE (Arendt et al. 1998). A much more extensive catalogue of ground based photometric observations was produced from 2MASS observations in the *J*, *H*, and *Ks* bands (Skrutskie et al. 2006). Observations at longer wavelengths have been performed by SPITZER ($> 5.3\,\mu m$), MSX ($> 8.3\,\mu m$), IRAS ($> 12\,\mu m$), AKARI ($> 50\,\mu m$), and Herschel ($> 55\,\mu m$). None of these instruments span the entire range accessible to VIMS and many of them have been unable to observe the brightest stars as they are beyond the instrumental saturation limit. VIMS has previously been used for stellar studies using stellar occultations by Saturn's rings (Stewart et al. 2013, 2014, 2015a,b,c), but until now has not been used for studies of stellar spectra.

The atlas provides unique access to broadband, space-based spectra of many of the brightest stars in the sky, albeit at a relatively low spectral resolution. This paper starts with a description of the experiment and instrument in Section 2, followed by details on the data reduction processes in Section 3. Sample spectra are presented in Section 4, and compared with those obtained by ISO and IRTF, and photometry from DIRBE and 2MASS. The full list of stars in the atlas is provided in Appendix A and reduced spectra are available online at `http://www.physics.usyd.edu.au/sifa/caoss/` and Vizier. By making these spectra available, we anticipate scientific benefits beyond the goals of the *Cassini* mission, and hope to enable new sections of the astronomical community to gain directly from a planetary exploration mission.

2. Experiment Description

The observations were originally acquired for the purposes of monitoring for any temporal variations within the VIMS instrument and to provide a baseline for the interpretation of stellar occultation results. Their acquisition started in the early stages of the mission, whilst the spacecraft was in "cruise" and on its way to Saturn, with the program expected to continue through to the end of the mission. The observations from this monitoring program were not intended to be used for stellar science. However, they fill a void in spectral coverage for a sufficient number of bright stars so as to warrant dissemination to the wider astronomical community.

2.1. The VIMS Instrument

VIMS was designed to observe the spatially resolved visible and near-infrared spectra of various surfaces in the Saturnian system. An overview of the instrumental design was

published by Brown et al. (2004) and the significant points will be reviewed here. The instrument has two independent, bore-sighted telescopes feeding separate visible and near-infrared spectrometers referred to as VIMS-VIS and VIMS-IR respectively. The diameters of these telescopes are 4.5 cm for the visible and 23 cm for the infrared, with the corresponding spectrometers spanning 0.35 - 1.05 μm in 96 channels and 0.8-5.1 μm in 256 channels. Both channels were operating when the observations used in this atlas were acquired, but due to the small collecting area of its telescope the visible channel generally did not yield sufficient signal to noise ratio to provide useful stellar spectra. Consequently, the information from the visible channel was not used in the preparation of this atlas, and only data from VIMS-IR is presented. VIMS-IR uses a triply-blazed diffraction grating with a spectrometer of conventional design with the spectral resolution (R) changing linearly from 53.5 at the blue end to 325 at the longest wavelength. The detector response was measured in ground tests prior to launch and was found to be entirely linear with incident flux. Due to its large spectral range, the infrared spectrometer employs a 4-element blocking filter to exclude higher-order transmissions from the diffraction grating; this results in small gaps in the spectra near 1.6, 3.0, and 3.9 μm due to the boundaries between the filter segments. The filter gap at 3.9 μm affects 4 spectral channels, whilst the other two gaps are each two spectral channels wide. Because of the 20-year duration of the *Cassini* mission, cryogens are impractical and VIMS is passively cooled via a radiator. The 256-element InSb alloy detector operates at a stable temperature of 58-60 K, but the spectrometer optics are typically at ~130 K. The instrumental thermal background is measured periodically during routine observations and subtracted from the target spectrum.

The VIMS instrument was designed to observe extended objects that entirely fill its instantaneous field of view, such as Saturn, its moons, and the ring system. Images are built up by measuring the spectrum of a single pointing individually and then moving the tip and tilt of the secondary mirror to raster in two dimensions over the required field. Each "pixel"

in this time-series image scan subtends a relatively large 228×493 μrad rectangular piece of the sky, with the tip and tilt of the secondary mirror providing a measured pixel centre separation of 250×500 μrad (Brown et al. 2004). This results in a photon collection area covering only ~90% of the image. The spacecraft pointing accuracy has been determined to be <629 μrad and the pointing stability has been measured to plateau below 6 μrad (Pilinski & Lee 2009). This is not a concern for existing VIMS observations within the Saturnian system which involve filled pixels, but it introduces problems when observing unresolved point-sources such as stars. As the pixel size is much larger than the stellar PSF, it is likely that ~10% of the time the stellar image will fall partially within these uncollected inter-pixel dead gaps in the 2D raster scan. In spite of this uncertainty in the precise position of the star within a pixel, drift in pointing over the duration of an observation is negligible. There are known to be small variations in the size and shape of this instrumental pixel as a function of wavelength. Observations in which the PSF falls substantially within these unmeasured inter-pixel dead zones are identified by fitting a modelled instrumental PSF to the observation (P. Stewart 2015 PhD Thesis in preparation). Such observations were found to be spectrally and photometrically inconsistent, and have been identified and removed from the main atlas.

McCord et al. (2004) show that under-filled pixels can effect the wavelength calibration by up to half a spectral channel (6-8 nm) and more recently there has been a report of a gradual monotonic drift in wavelength of up to 9 nm toward the red since the spacecraft's launch (NASA PDS 2015b). This has been incorporated into the wavelength uncertainty discussed in Section 3.1.

VIMS-IR images used in this project have been acquired in one of two imaging modes, known as NORMAL and HIRES. The NORMAL mode co-adds two adjacent rectangular pixels to produce square pixels, whilst HIRES keeps the instrumental rectangular pixels to

produce higher resolution images in one dimension. The two modes have been shown to provide consistent spectra, and data have been averaged together where observations in both modes exist.

3. Data Reduction Process

The observations were obtained from the data archive at the Planetary Rings Node of NASA's Planetary Data System (PDS) (NASA PDS 2015a). The raw format stores the intensity across the spectrum in background-subtracted detector counts together with the background itself. The parameters of the observation and instrumental operation are recorded in the data file headers.

These observations were performed in the raster-scanning mode described above and stored as 3D image "cubes". The full 0.8-5.1 μm spectrum was obtained simultaneously for each signal pixel individually, with typical integration times of 320 or 640 ms per pixel. The images recorded by VIMS usually cover a 8x8 or 12x12 pixel field in all 352 spectral channels using measurements from both VIMS-VIS and VIMS-IR, but only the 256 channels recorded by the infrared instrument are used here. From the recorded data (Figure 1a), VIMS subtracts the measured background (Figure 1b) before transmitting them both back to Earth. The first step in the extraction of the stellar spectra from these cubes is to sum over a 3x3 pixel square, centred on the brightest pixel, producing a base spectral measurement as shown in Figure 1c. In order to determine if any spectral channels saturated during the exposure, the measured and separately recorded background spectrum (Figure 1b) is added to the brightest pixel's counts (Figure 1a). Any spectral channels which now show 4095 counts are flagged as saturated and are omitted. These occur frequently at the hot pixels shown as spikes in Figure 1b, such as the saturated pixel at 1.25 μm in Figure 1a. Similarly, pixels affected by cosmic rays are identified and flagged for omission. These base spectra

are divided by the geometric area of the telescope's aperture and the exposure time of the observation (extracted from data headers) to give the measured spectra in counts/m^2/s. The instrumental sensitivity function (Figure 1d), combining both the electronic gain and the detector sensitivity as a function of wavelength, is used to convert this into photons/m^2/s (Figure 1e). By dividing by the instrumental bandpass shown in Figure 1f ($\Delta\lambda$), we arrive at a spectrum in photons/m^2/s/μm (Figure 1g) which is multiplied by the photon energy (Figure 1h) to give J/m^2/s/μm. Finally this is converted into Janskys as shown in Figure 1i ($= 10^{-26} W m^{-2} H z^{-1}$) in order to compare with previously published spectra from the literature.

The sensitivity and bandpass functions were derived as part of the VIMS-IR calibration for extended sources. Clark et al. (2012) details the development of these functions through to the latest version (RC17) which is used in this work. For stellar sources which do not fill the spectrometer's pixel, the sensitivity function is expected to differ somewhat from these standard values. A wavelength-dependant systematic deviation between the recovered VIMS spectra and those previously published was noted in this work, and was found to be consistent across a range of stars of various types and spanning multiple epochs. A correction ratio was constructed based on a comparison of VIMS spectra for standard stars to corresponding literature spectra from Engelke et al. (2006) and Rayner et al. (2009). The ratios of sections of the literature spectra to VIMS observations were averaged to produce a mean brightness ratio by which VIMS observations were multiplied. Variable stars known to exhibit strong wavelength-dependent temporal variations which have the potential to introduce spectral artefacts, and those with an amplitude of greater than one magnitude in any part of the near infrared have been omitted. These relevant reference spectra are summarised in Table 1. The final correction function is available online with the atlas, and is provided to enable the application of alternative calibrations.

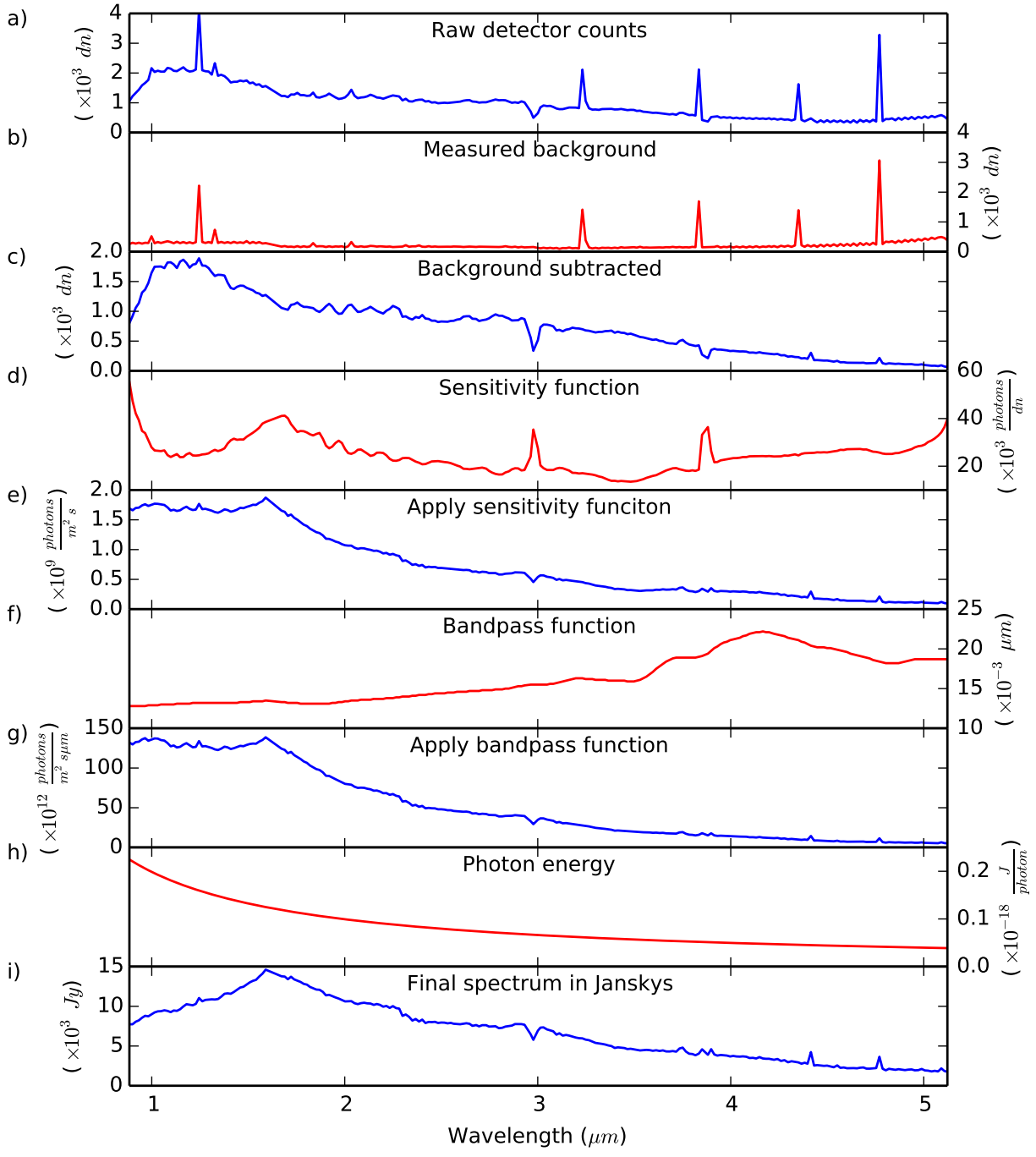

Fig. 1.— The data reduction process illustrated for a single 320 ms exposure of α Boo in sequence C34. The blue curves show the data progressing through the reduction process, whilst the requisite calibration curves are in red. Full details of each panel are in Section 3.

Figure 2 demonstrates the effectiveness of this correction as applied to α Boo from sequence S16. The resultant corrected spectrum provides a good match to the general shape of the literature data, as well as some of the finer details, especially through 2.2-2.6 μm and the narrow absorption feature near 1.1 μm. For comparison purposes, the literature spectra have been downsampled to match the spectral resolution of VIMS. In order to to ensure the robustness of this comparison we also produced a calibration curve omitting the 'test' epoch and found the resultant curve to be indistinguishable from that produced using all observations which have literature spectra. Application of this correction function is only necessary when observing point-sources, and calibrating filled-pixel spectra does not require this step.

The spectra are presented without any correction for interstellar reddening for the following reasons. The majority of sources in the atlas are close to the Sun and thus have A_V values of approximately zero, with half the sample within 110 pc and only 10 stars further than 500 pc. Extinction corrections are much smaller in the infrared than in the optical, reducing the impact of interstellar reddening on stars in the atlas. It is not envisioned that the calibration pipeline presented here will change, whereas extinction corrections, dependent on poorly known distances and estimated extinctions to that distance along a given line-of-sight, will almost certainly change in the future. This is especially likely as 3D extinction models of the Galaxy improve over the coming decades.

Table 1: A table of observations used to derive the calibration correction ratio. The first set of data are derived from space-based ISO SWS observations, whilst the second set originate from terrestrial observations performed with IRTF. Epochs are in *Cassini* planning sequences, and are available in UTC and Julian dates in Table 4.

λ (μm)	Stars Used (Epochs)	Source for Ref. Spectrum
2.4 - 5.1	alp Boo (C27, C34, S36)	Engelke et al. (2006)
	alp Tau (C35)	”
	bet UMi (S35)	”
	alp Cet (S18)	”
	bet And (S18)	”
	gam Cru (C35, S38, S53)	”
	alp CMa (C39, S69)	”
0.8 - 2.4	alp Boo (C27, C34, S36)	Rayner et al. (2009)
	alp Ori (C33, S18)	”
	mu Cep (S22)	”
	R Lyr (S13, S79)	”
	alp Her (S13, S53)	”
	rho Per (S18)	”

3.1. Data Products

Spectra are identified by the name of the stellar target and the mission sequence in which they were observed. These sequences are labelled either "C" or "S" identifying either "cruise" or "Saturnian orbit". They are then numbered sequentially with time with each "S" sequence spanning several planetary orbits by the spacecraft. As an example, RDor C33 is a spectrum of the star R Doradus observed in the 33rd cruise sequence. The UTC and Julian dates of these are included in Table 4, as are the number of exposures and cumulative integration time of all exposures for each observation.

Each spectrum presented is the average of all frames acquired within a given observation. The actual UTC date and time of each of the averaged exposures is included in the data header, along with the exposure times, image dimensions, and instrument mode. The final data products are available as simple text files, and as four column fits tables, with the columns being centre wavelength, flux density, uncertainty in centre wavelength and uncertainty in flux density.

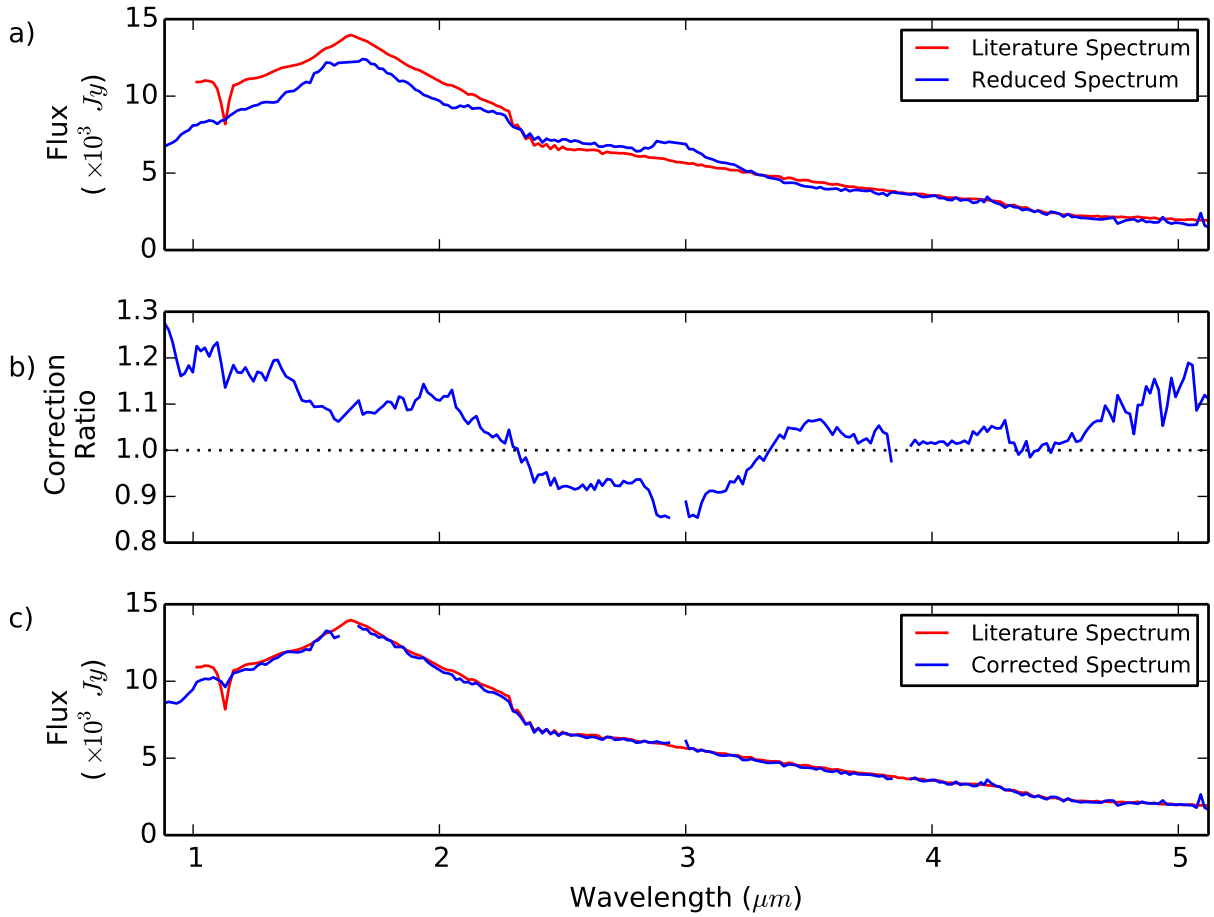

Fig. 2.— A demonstration of the effectiveness of the correction function discussed in Section 3 on the S16 observation of α Boo. Panel (a) shows a comparison of the processed VIMS spectrum (in blue) against a published spectrum from Engelke et al. (2006), resampled to the same spectral resolution. Panel (b) shows the correction ratio by which all VIMS stellar spectra are multiplied to produce a corrected spectrum. The final panel (c) shows the corrected VIMS spectrum against the resampled Engelke et al. (2006) curve.

Table 2: The number of stars of each spectral class and variability type in CAOSS

By Spectral Class	O	1
	A	2
	F	2
	C	3
	S	3
	K	8
	M0-4	17
	M5-9	29
By Variability Type	Irregular	13
	Mira	16
	Semiregular	20

Table 3 includes optical spectral classes for each source, based on a review of the classification literature. We generally report the oldest classification(s) consistent with subsequent papers, except where improved classifications are available from Morgan & Keenan (1973), Keenan et al. (1974), or Keenan & McNeil (1989). Sloan et al. (2015) report spectral types for 14 targets in the CAOSS sample, based on slightly different rules, and as a consequence several differ by a step in spectral class or luminosity class. These differences indicate the level of uncertainty in the classifications. We do not report spectral types for optical companions which do not contribute significantly to the near-infrared spectrum.

4. Sample Spectra

The spectra produced in this work include stars from many spectral classes including A and G main sequence stars and K giants, but due to engineering requirements for bright targets, the atlas is dominated by evolved M giants. Many of these targets have complex molecular atmospheres and exhibit variability. This section shows some of the recovered spectra and compares them, where possible, to existing literature measurements. These literature values come predominately from space-based ISO SWS spectra (Engelke et al. 2006) and ground-based IRTF spectra (Rayner et al. 2009), with space-based photometry from DIRBE (Arendt et al. 1998). WISE photometry was found to be unreliable for many of these targets due to unflagged saturation. For accurate comparison, both the ISO and IRTF spectra have been downsampled to match the spectral resolution of VIMS.

To give a sample of the CAOSS data, Figure 3 shows reduced spectra for five different stellar targets. Each panel labelled (a) to (e), contains an observation at a single epoch for a single star. Panel (a) shows the A1 star Sirius (α Canis Majoris) with a spectrum comprising predominately the Rayleigh-Jeans side of a hot Planck curve (Sirius has an effective surface temperature of approximately 10,000 K with peak intensity in the ultraviolet). This shows

very good agreement with the Engelke et al. (2006) spectrum, as well as both the DIRBE and 2MASS photometry. Panel (b) contains the blended spectrum of the binary system, α Centauri A and B and also shows good agreement to the 2MASS photometry. Panels (c) and (d) contain the early-mid M giants ρ Persei and γ Crucis. These spectra have broadly similar shapes, yet very different magnitudes due to the latter's relative proximity. They agree well with existing literature spectra and photometry from all four sources. The final panel (e), shows R Cnc, a Mira variable type star with a spectral class of M6.5-9. Such stars are known to exhibit huge variations in magnitude over a period on the order of a year. The spectrum presented only partly agree with the published Rayner et al. (2009) IRTF spectra and 2MASS photometry, which in keeping with the known spectral variability of such objects.

Figure 4 shows two more Mira variable stars for which there are multiple epochs presented in this atlas. Large changes in overall flux, accompanied by more minor shifts in spectral shape are noted between epochs. The variations in flux for these particular stars, as with all variable stars in the atlas, have been checked against the AAVSO lightcurves and found to be broadly consistent, but no detailed analysis of stellar variability has been performed in this work.

5. Conclusions

We have produced a database of space-based near-infrared spectra for 73 stellar targets at 109 epochs. These spectra have been made publicly available online in flexible data formats. Where comparison was possible they have been shown to be consistent with existing spectra and photometry. In spite of the relatively low spectral resolution, we believe that these spectra are of sufficient quality to continuously bridge a vital yet unsurveyed part of the spectrum and to become a valuable resource for the stellar astrophysical community.

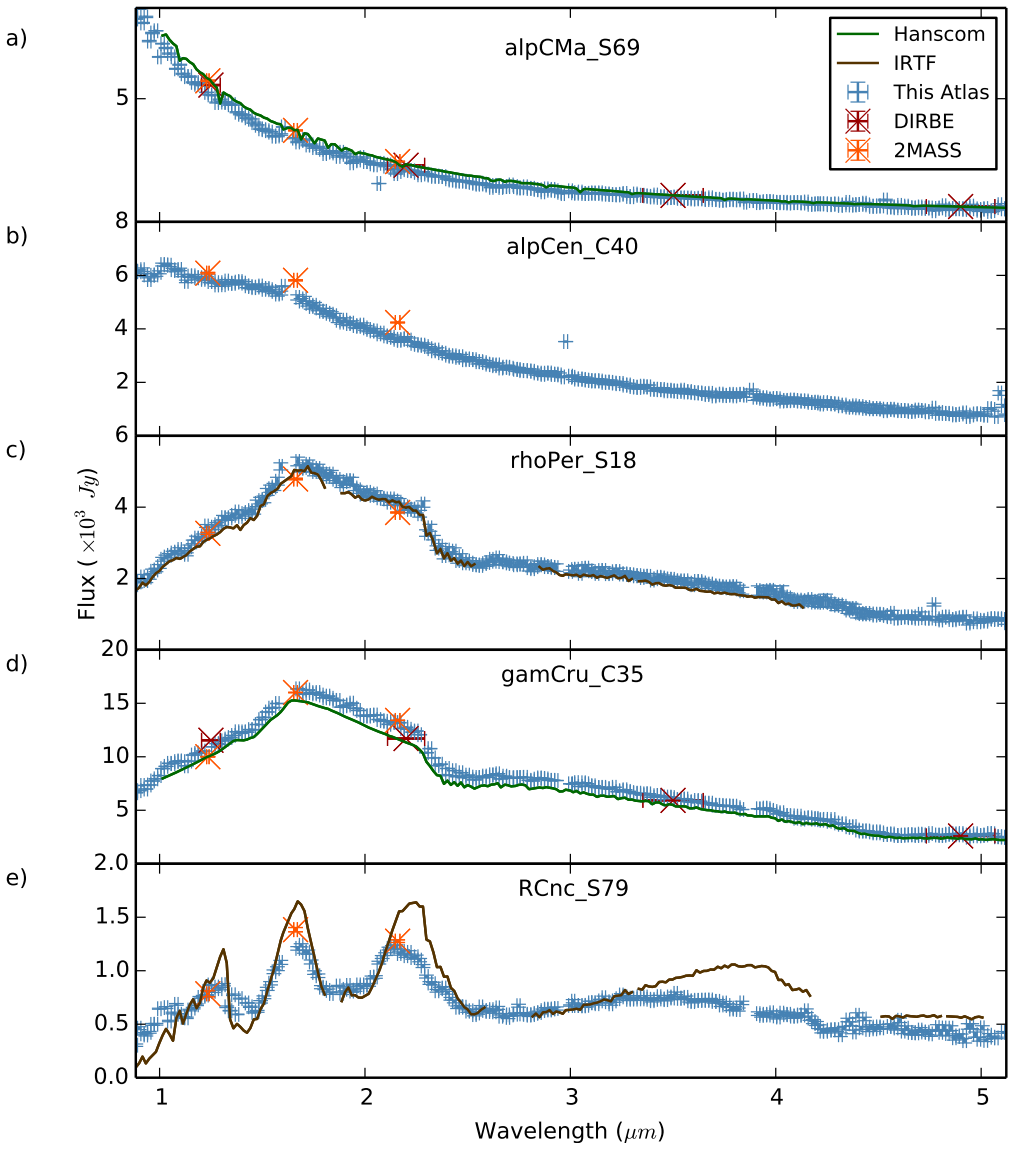

Fig. 3.— A comparison of spectra presented in this atlas (blue) to the literature. The vertical axis is stellar flux density in 10^3 Janskys and the horizontal axis is wavelength in microns. Spectra of Hansom standard stars from ISO by Engelke et al. (2006) are shown as green curves and IRTF spectra by Rayner et al. (2009) are rendered as brown curves. Photometric measurements are shown as individual points with error bars in dark red and orange for DIRBE and 2MASS, respectively. The discrepancy in panel (e) is due to the inherently variable nature of the target star, R Cnc.

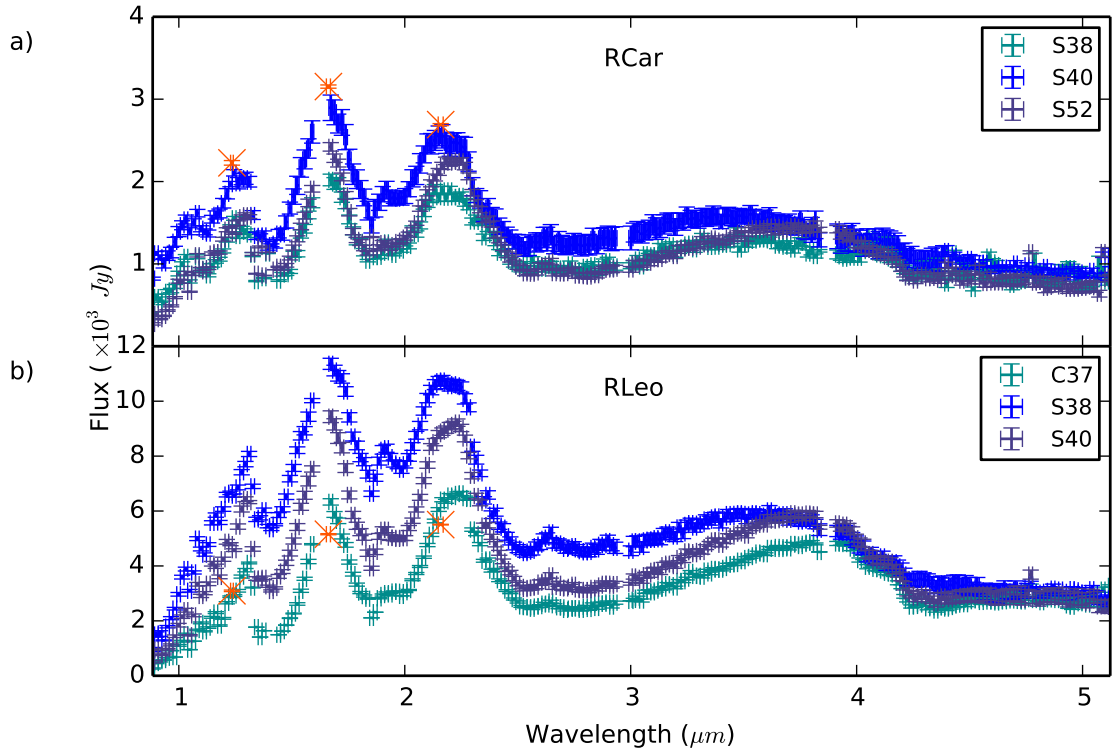

Fig. 4.— Multiple epochs of variable stars showing significant temporal variation. Each panel shows a spectrum for the three epochs indicated in the legend. The orange points show 2MASS photometry from an epoch independent of the VIMS observations.

As spectra from this dataset span the telluric water bands they particularly enable the study of evolved stars, known to exhibit strong spectral structure from their own atmospheric water. Spectra presented in this atlas have already been used in a study of the atmosphere of Mira, including an assessment of models of its atmospheric behaviour (Stewart et al. 2015c).

Acknowledgements

This research made use of the SIMBAD database, operated at CDS, Strasbourg, France.

Some of the data presented in this paper were obtained from the Mikulski Archive for Space Telescopes (MAST). STScI is operated by the Association of Universities for Research in Astronomy, Inc., under NASA contract NAS5-26555. Support for MAST for non-HST data is provided by the NASA Office of Space Science via grant NNX13AC07G and by other grants and contracts.

This publication makes use of data products from the Two Micron All Sky Survey, which is a joint project of the University of Massachusetts and the Infrared Processing and Analysis Center/California Institute of Technology, funded by the National Aeronautics and Space Administration and the National Science Foundation.

REFERENCES

Adams, W. S., Joy, A. H., & Humason, M. L. 1926, ApJ, 64, 225

Arendt, R. G., Berriman, G. B., Franz, B. A., et al. 1998, COBE Diffuse Infrared Background Experiment (DIRBE) Explanatory Supplement, 2nd edn., ed. M. G. Hauser, T. Kelsall, D. Leisawitz, & J. Weiland, 79–85

Bidelman, W. P. 1954, ApJS, 1, 175

—. 1985, ApJS, 59, 197

Boggess, A., Carr, F. A., Evans, D. C., et al. 1978, Nature, 275, 372

Brown, R. H., Baines, K. H., Bellucci, G., et al. 2004, Space Science Reviews, 115, 111

Clark, R. N., Cruikshank, D. P., Jaumann, R., et al. 2012, Icarus, 218, 831

Cohen, M. 1979, MNRAS, 186, 837

de Graauw, T., Haser, L. N., Beintema, D. A., et al. 1996, A&A, 315, L49

Eggen, O. J. 1960, MNRAS, 120

Engelke, C. W., Price, S. D., & Kraemer, K. E. 2006, AJ, 132, 1445

Evans, D. S. 1957, Monthly Notes of the Astron. Soc. Southern Africa, 16

Gascoigne, S. C. B. 1950, MNRAS, 110

Greenstein, J. L. 1948, ApJ, 107, 151

Høg, E., Fabricius, C., Makarov, V. V., et al. 2000, A&A

Houk, N., & Cowley, A. P. 1975, University of Michigan Catalogue of two-dimensional spectral types for the HD stars, Vol. I

Hoyle, F., & Wilson, O. C. 1958, ApJ, 128, 604

Humphreys, R. M., Strecker, D. W., & Ney, E. P. 1972, ApJ, 172, 75

Joy, A. H. 1926, ApJ, 63, 281

Keenan, P. C. 1942, ApJ, 95, 461

Keenan, P. C., & Boeshaar, P. C. 1980, ApJS, 43, 379

Keenan, P. C., Garrison, R. F., & Deutsch, A. J. 1974, ApJS, 28, 271

Keenan, P. C., & Hynek, J. A. 1945, ApJ, 101, 265

Keenan, P. C., & McNeil, R. C. 1989, ApJS, 71, 245

Landi Dessy, J., & Keenan, P. C. 1966, ApJ, 146, 587

Loup, ., Forveille, ., Omont, ., & Paul, . 1993, Astronomy and Astrophysics Supplement Series (ISSN 0365-0138), 99, 291

McCord, T. B., Coradini, A., Hibbitts, C. A., et al. 2004, Icarus, 172, 104

Morgan, W. W., Harris, D. L., & Johnson, H. L. 1953, ApJ, 118, 92

Morgan, W. W., & Keenan, P. C. 1973, ARA&A, 11, 29

Morgan, W. W., Keenan, P. C., & Kellman, E. 1943, An atlas of stellar spectra, with an outline of spectral classification (Chicago, Ill., The University of Chicago press)

NASA PDS. 2015a, The Rings Node of NASA's Planetary Data System *http://pds-rings.seti.org/*

—. 2015b, VIMS - Visual and Infrared Mapping Spectrometer : PDS: The Planetary Atmospheres Data Node *http://atmos.nmsu.edu/data_and_services/atmospheres_data/Cassini/vims.html*

Pesch, P. 1967, ApJ, 147, 381

Pilinski, E. B., & Lee, A. Y. 2009, Journal of Spacecraft and Rockets, 46, 1007

Rayner, J. T., Cushing, M. C., & Vacca, W. D. 2009, The Astrophysical Journal Supplement Series, 185, 289

Roman, N. G. 1952, ApJ, 116, 122

Samus, N. N., Durlevich, O. V., & al., E. 2009, VizieR On-line Data Catalog: B/gcvs.

Sanford, R. F. 1944, ApJ, 99, 145

Skrutskie, M. F., Cutri, R. M., Stiening, R., et al. 2006, AJ, 131, 1163

Sloan, G. C., Goes, C. W., Ramirez, R. M., Kraemer, K. E., & Engelke, C. W. 2015, ApJ, 811, 45

Stewart, P. N., Tuthill, P. G., Hedman, M. M., Nicholson, P. D., & Lloyd, J. P. 2013, MNRAS, 433, 2286

Stewart, P. N., Tuthill, P. G., Monnier, J. D., et al. 2015a, MNRAS, Accepted, doi:10.1093/mnras/stv2454

Stewart, P. N., Tuthill, P. G., Nicholson, P. D., & Hedman, M. M. 2015b, MNRAS, Submitted

Stewart, P. N., Tuthill, P. G., Nicholson, P. D., Hedman, M. M., & Lloyd, J. P. 2014, in Proc. SPIE, 91431G

Stewart, P. N., Tuthill, P. G., Nicholson, P. D., Hedman, M. M., & Lloyd, J. P. 2015c, MNRAS, 449, 1760

Teodoro, M., Damineli, A., Sharp, R. G., Groh, J. H., & Barbosa, C. L. 2008, MNRAS, 387, 564

Thompson, R. I., Rieke, M., Schneider, G., Hines, D. C., & Corbin, M. R. 1998, ApJ, 492, L95

van Leeuwen, F. 2007, A&A, 474, 653

Wilson, O. C., & Vainu Bappu, M. K. 1957, ApJ, 125, 661

Wing, F. R., & Lockwood, G. W. 1973, ApJ, 184, 873

Woodgate, B. E., Kimble, R. A., Bowers, C. W., et al. 1998, PASP, 110, 1183

Woolley, R. V. D. R., Gottlieb, K., & Przybylski, A. 1952, MNRAS, 112

Yamashita, Y. 1967, Publications of the Dominion Astrophysical Observatory, 13

A. The *Cassini* Atlas Of Stellar Spectra

The details of all stars contained in CAOSS are listed in Table 3, including coordinates, spectral type and variability type where relevant. A full list of flux density calibrated spectra to date is contained in Table 4. Observations processed identically to those in Table 4 yet containing significant deviations from the literature values are presented online with the atlas, but not listed here. These spectra are still expected to be of value in situations where an absolute flux density calibration is not required.

This manuscript was prepared with the AAS LaTeX macros v5.2.

Table 3:: Stars in the Cassini Atlas of Stellar Spectra. Details of individual observations are listed in Table 4.

Target			R.A. Declination	Parallax	ePlx	Spectral	Spectral	Var.
Name	HIP	Alias	(J2000)[a]	(mas)		Type	Reference[b]	Class[c]
30 Psc	154	YY Psc	00 01 57.62 -06 00 50.66	7.55	0.59	M3 III	M73	Lb:
bet And	5447	–	01 09 43.92 +35 37 14.01	16.52	0.56	M0 III var	M43	nsv
gam1 And	9640	–	02 03 53.95 +42 19 47.02	8.3	1.04	K3 II	M73	–
omi Cet	10826	–	02 19 20.79 -02 58 39.50	10.91	1.22	M5-M9e	J26	Mira
alp Cet	14135	–	03 02 16.77 +04 05 23.06	13.09	0.44	M1.5 IIIa	K89	Lb:
rho Per	14354	–	03 05 10.59 +38 50 24.99	10.6	0.25	M3 II-III	M73	SRb
NML Tau	–	IK Tau	03 53 28.87 +11 24 21.70	–	–	M9	P67	Mira
gam Eri	18543	–	03 58 01.77 -13 30 30.67	16.04	0.58	M0 III-IIIb	K89	Lb:
alp Tau	21421	–	04 35 55.24 +16 30 33.49	48.94	0.77	K5 III	M43, R52	Lb:
R Dor	21479	–	04 36 45.59 -62 04 37.80	18.31	0.99	M8e	M73	SRb
TX Cam	–	–	05 00 50.39 +56 10 52.60	–	–	M8-10	W73	Mira
RX Lep	24169	–	05 11 22.87 +05 09 02.75	6.71	0.44	M6 III	A26	SRb
alp Aur	24608	Capella	05 16 41.35 +45 59 52.80	76.2	0.46	G1 III+K0 III	Simbad	nsv
alp Ori	27989	–	05 55 10.31 +07 24 25.43	6.55	0.83	M1.5 Iab	M73	SRc
mu Gem	30343	–	06 22 57.63 +22 30 48.90	14.08	0.71	M3 IIIab	K89	Lb

Continued on next page

Table 3 – continued from previous page

Name	Target HIP	Alias	R.A. Declination (J2000)[a]	Parallax (mas)	ePlx	Spectral Type	Spectral Reference[b]	Var. Class[c]
alp Car	30438	–	06 23 57.11 -52 41 44.38	10.55	0.56	F0 II	G48	–
alp CMa	32349	–	06 45 08.92 -16 42 58.02	379.21	1.58	A1 V	M43	nsv
L2 Pup	34922	–	07 13 32.32 -44 38 23.06	15.61	0.99	M5 IIIe	B85	SRb
VY CMa	35793	–	07 22 58.33 -25 46 03.24	–	–	M5 Iae	H72	–
sig Pup	36377	–	07 29 13.83 -43 18 05.16	16.84	0.48	K5 III	E57	Ell:
alp CMi	37279	–	07 39 18.12 +05 13 29.96	284.56	1.26	F5 IV	G48	nsv
R Cnc	40534	–	08 16 33.83 +11 43 34.46	1.58	1.43	M6.5-9e	K74	Mira
lam Vel	44816	–	09 07 59.76 -43 25 57.33	5.99	0.11	K4 Ib	K89	Lc
RS Cnc	45058	–	09 10 38.80 +30 57 47.30	6.97	0.52	M6S	B54	SRc:
alp Hya	46390	–	09 27 35.24 -08 39 30.96	18.09	0.18	K3 II-III	M73	nsv
R Car	46806	–	09 32 14.60 -62 47 19.97	6.34	0.81	M8e III:	K89	Mira
R Leo	48036	–	09 47 33.49 +11 25 43.66	14.03	2.65	M7-9e	K74	Mira
CW Leo	–	IRC+10216	09 47 57.41 +13 16 43.68	–	–	C9	Simbad	M
RW LMi	–	CIT 6	10 16 02.27 +30 34 18.60	–	–	C4,3e	C79	SRa
U Ant	51821	–	10 35 12.85 -39 33 45.32	3.73	0.54	C5,4	S44	Lb
eta Car	–	–	10 45 03.55 -59 41 03.95	–	–	O5.5 III - O7 I	T08	S Dor

Continued on next page

Table 3 – continued from previous page

Target Name	HIP	Alias	R.A. Declination (J2000)[a]	Parallax (mas)	ePlx	Spectral Type	Spectral Reference[b]	Var. Class[c]
V Hya	53085	–	10 51 37.26 -21 15 00.32	1.44	1.41	C7.5e	B54	SRa
56 Leo	53449	VY Leo	10 56 01.47 +06 11 07.33	8.39	0.37	M5.5 III	M73	Lb:
ome Vir	56779	–	11 38 27.61 +08 08 03.47	6.56	0.36	M4.5: III	K89	Lb
nu Vir	57380	–	11 45 51.56 +06 31 45.74	11.1	0.18	M1 III	M73	SRb
eps Mus	59929	–	12 17 34.28 -67 57 38.65	10.82	0.17	M5 III	L66	SRb:
gam Cru	61084	–	12 31 09.96 -57 06 47.57	36.83	0.18	M3.5 III	K89	nsv
del Vir	63090	–	12 55 36.21 +03 23 50.89	16.44	0.22	M3 III	W57, H58	nsv
R Hya	65835	–	13 29 42.78 -23 16 52.77	8.05	0.69	M6.5-9e	K74	Mira
W Hya	67419	–	13 49 02.00 -28 22 03.49	9.59	1.12	M7.5-9e	K74	SRa
2 Cen	67457	V806 Cen	13 49 26.72 -34 27 02.79	17.82	0.21	M4.5 IIIb	L66	SRb
alp Boo	69673	–	14 15 39.67 +19 10 56.67	88.83	0.54	K1.5 III	K89	nsv
alp Cen B	71681	–	14 39 35.06 -60 50 15.10	796.92	25.9	K1 V	H75	–
alp Cen A	71683	–	14 39 36.49 -60 50 02.37	754.81	4.11	G2 V	G50	–
bet UMi	72607	–	14 50 42.33 +74 09 19.81	24.91	0.12	K4 III var	R52, M53	nsv
RR UMi	73199	–	14 57 35.01 +65 55 56.86	7.1	0.37	M4.5 III	K89	SRb
R Ser	77615	–	15 50 41.74 +15 08 01.10	4.78	1.84	M5-7e	K74	Mira

Continued on next page

Table 3 – continued from previous page

Name	Target HIP	Alias	R.A. Declination (J2000)[a]	Parallax (mas)	ePlx	Spectral Type	Spectral Reference[b]	Var. Class[c]
del Oph	79593	–	16 14 20.74 -03 41 39.56	19.06	0.16	M0.5 III	M73	nsv
U Her	80488	–	16 25 47.47 +18 53 32.86	4.26	0.85	M8e	K74	Mira
30 Her	90704	g Her	16 28 38.55 +41 52 54.04	9.21	0.18	M6 III	M73	SRb
alp Sco	80763	–	16 29 24.46 -26 25 55.21	5.89	1.0	M1.5 Iab	M73	Lc
alp TrA	82273	–	16 48 39.89 -69 01 39.76	8.35	0.15	K2 III	W52	–
alp Her	84345	–	17 14 38.86 +14 23 25.08	0.07	1.32	M5 II	W57	SRc
alp Her A	84345	–	17 14 38.86 +14 23 25.23	9.07	1.32	M5 Ib-II	M73	SRc
VX Sgr	88838	–	18 08 04.05 -22 13 26.63	3.82	2.73	M4 Iae	H72	SRc
eta Sgr	89642	–	18 17 37.64 -36 45 42.07	22.35	0.24	M3 II	O60	Lb:
alp Lyr	91262	–	18 36 56.33 +38 47 01.32	130.23	0.36	A0 Va	Simbad	DSCTC
X Oph	91389	–	18 38 21.12 +08 50 02.75	–	–	M0-8e + K2: III	K74	Mira
R Lyr	92862	–	18 55 20.10 +43 56 45.93	10.94	0.12	M5 III var	K45	SRb
R Aql	93820	–	19 06 22.25 +08 13 48.01	2.37	0.87	M6.5-9e	K74	Mira
W Aql	–	–	19 15 23.35 -07 02 50.35	–	–	S6/6e	K80	Mira
chi Cyg	97629	–	19 50 33.92 +32 54 50.61	5.53	1.1	S6-9/1-2e	K80	Mira
T Cep	104451	–	21 09 31.78 +68 29 27.20	5.33	0.9	M6-9e	K74	Mira

Continued on next page

Table 3 – continued from previous page

Name	Target HIP	Alias	R.A. Declination (J2000)[a]	Parallax (mas)	ePlx	Spectral Type	Spectral Reference[b]	Var. Class[c]
W Cyg	106642	–	21 36 02.50 +45 22 28.53	5.72	0.38	M5+ IIIa	Y67	SRb
mu Cep	107259	–	21 43 30.46 +58 46 48.16	0.55	0.2	M2 Ia	K42	SRc
pi1 Gru	110478	–	22 22 44.21 -45 56 52.61	6.13	0.76	S5,7:	B54	SRb
bet Gru	112122	–	22 42 40.05 -46 53 04.48	18.43	0.42	M4.5 III	K89	Lc:
lam Aqr	112961	–	22 52 36.86 -07 34 46.56	8.47	0.66	M2 III	Simbad	LB
alp PsA	113368	–	22 57 39.05 -29 37 20.05	129.81	0.47	A3 V	M43	nsv
bet Peg	113881	–	23 03 46.46 +28 04 58.03	16.64	0.15	M2.5 II-III	M73	Lb
chi Aqr	114939	–	23 16 50.93 -07 43 35.40	5.32	0.37	M3 III	Simbad	–
R Aqr	117054	–	23 43 49.46 -15 17 04.14	2.76	2.27	M6.5-9ep	K74	Mira
R Cas	118188	–	23 58 24.87 +51 23 19.70	7.95	1.02	M6-9e	K74	Mira

[a] Coordinates and parallaxes from van Leeuwen (2007), except for eta Car and VY CMa (Høg et al. 2000), NML Tau (Skrutskie et al. 2006), and RW LMi and TX Cam (Loup et al. 1993).

[b] References are meant to be representative: A26 (Adams et al. 1926), B54 (Bidelman 1954), B85 (Bidelman 1985), C79 (Cohen 1979), E57 (Evans 1957), E60 (Eggen 1960), G48 (Greenstein 1948), G50 (Gascoigne 1950), H58 (Hoyle & Wilson 1958), H72 (Humphreys et al. 1972), H75 (Houk & Cowley 1975), J26 (Joy 1926), K42 (Keenan 1942), K45 (Keenan & Hynek 1945), K74 (Keenan et al. 1974), K80 (Keenan & Boeshaar 1980), K89 (Keenan & McNeil 1989), L66 (Landi Dessy & Keenan 1966), M43 (Morgan et al. 1943), M53 (Morgan et al. 1953), M73 (Morgan & Keenan 1973), P67 (Pesch 1967), R52 (Roman 1952), S44 (Sanford 1944), T08 (Teodoro et al. 2008), W52 (Woolley et al. 1952), W57 (Wilson & Vainu Bappu 1957), W73 (Wing & Lockwood 1973), Y67 (Yamashita 1967).

[c] Variability Class is from the General Catalog of Variable Stars (Samus et al. 2009).

Table 4:: The Cassini Atlas of Stellar Spectra. All epochs listed are where flux calibrated spectra were recovered. The columns from left to right are: name of the stellar target, R.A. and Dec from Table 3, Cassini planning sequence, UTC and Julian dates, number of exposures, and cumulative exposure time per pixel. Sorted by Right Ascension.

Target	R.A. Declination (J2000)	Sequence	Epoch		No. of Exp.	Total Exp. Time (s)
			UTC	JD		
30 Psc	00 01 57.62 -06 00 50.66	S25	2006-11-5	2454044	15	4.7
bet And	01 09 43.92 +35 37 14.01	S18	2006-2-1	2453767	15	4.7
gam1 And	02 03 53.95 +42 19 47.02	S18	2006-2-1	2453767	15	4.7
omi Cet	02 19 20.79 -02 58 39.50	S83	2014-4-11	2456758	29	18.1
alp Cet	03 02 16.77 +04 05 23.06	S18	2006-2-1	2453767	14	4.1
rho Per	03 05 10.59 +38 50 24.99	S18	2006-2-1	2453767	21	5.0
NML Tau	03 53 28.87 +11 24 21.70	C33	2002-7-19	2452474	22	15.1
gam Eri	03 58 01.77 -13 30 30.67	S27	2007-2-16	2454147	14	4.1
alp Tau	04 35 55.24 +16 30 33.49	C35	2003-1-19	2452658	40	20.2
R Dor	04 36 45.59 -62 04 37.80	C33	2002-7-18	2452473	82	54.3
TX Cam	05 00 50.39 +56 10 52.60	S27	2007-2-15	2454146	16	5.4
RX Lep	05 11 22.87 +05 09 02.75	S27	2007-2-16	2454147	14	4.1
alp Ori	05 55 10.31 +07 24 25.43	S18	2006-2-1	2453767	20	1.9
mu Gem	06 22 57.63 +22 30 48.90	S18	2006-2-1	2453767	19	3.1
alp Car	06 23 57.11 -52 41 44.38	C34	2002-10-19	2452566	39	7.8
alp Car	06 23 57.11 -52 41 44.38	S69	2011-7-27	2455769	260	44.7
alp CMa	06 45 08.92 -16 42 58.02	C39	2003-10-13	2452925	43	12.9
alp CMa	06 45 08.92 -16 42 58.02	S69	2011-7-27	2455769	15	8.3

Continued on next page

Table 4 – continued from previous page

Target	R.A. Declination (J2000)	Sequence	Epoch UTC	Epoch JD	No. of Exp.	Total Exp. Time (s)
L2 Pup	07 13 32.32 -44 38 23.06	S36	2008-1-12	2454477	14	2.2
VY CMa	07 22 58.33 -25 46 03.24	S36	2008-1-12	2454477	7	2.5
sig Pup	07 29 13.83 -43 18 05.16	S83	2014-5-1	2456778	52	30.7
alp CMi	07 39 18.12 +05 13 29.96	S08	2005-1-30	2453400	15	4.7
R Cnc	08 16 33.83 +11 43 34.46	S79	2013-7-5	2456478	48	30.5
lam Vel	09 07 59.76 -43 25 57.33	S36	2008-1-12	2454477	9	2.6
RS Cnc	09 10 38.80 +30 57 47.30	S36	2008-1-12	2454477	14	2.8
RS Cnc	09 10 38.80 +30 57 47.30	S79	2013-7-5	2456478	48	30.5
alp Hya	09 27 35.24 -08 39 30.96	S35	2007-12-7	2454441	11	4.1
alp Hya	09 27 35.24 -08 39 30.96	S38	2008-3-9	2454534	8	3.2
alp Hya	09 27 35.24 -08 39 30.96	S81	2013-12-20	2456646	160	50.6
R Car	09 32 14.60 -62 47 19.97	S38	2008-2-27	2454523	6	1.9
R Car	09 32 14.60 -62 47 19.97	S40	2008-4-26	2454582	26	10.1
R Car	09 32 14.60 -62 47 19.97	S52	2009-8-1	2455044	32	12.7
R Leo	09 47 33.49 +11 25 43.66	C37	2003-5-19	2452778	47	9.5
R Leo	09 47 33.49 +11 25 43.66	S38	2008-3-3	2454528	20	5.4
R Leo	09 47 33.49 +11 25 43.66	S40	2008-4-26	2454582	30	10.5
R Leo	09 47 33.49 +11 25 43.66	S81	2013-12-20	2456646	160	50.6
RW LMi	10 16 02.27 +30 34 18.60	S08	2005-1-30	2453400	9	3.3
U Ant	10 35 12.85 -39 33 45.32	S84	2014-6-29	2456837	117	74.4
eta Car	10 45 03.55 -59 41 03.95	C33	2002-7-18	2452473	58	39.0
eta Car	10 45 03.55 -59 41 03.95	S38	2008-2-27	2454523	8	3.2

Continued on next page

Table 4 – continued from previous page

Target	R.A. Declination (J2000)	Sequence	Epoch UTC	Epoch JD	No. of Exp.	Total Exp. Time (s)
eta Car	10 45 03.55 -59 41 03.95	S81	2013-12-27	2456653	85	54.1
V Hya	10 51 37.26 -21 15 00.32	S28	2007-2-25	2454156	35	10.6
56 Leo	10 56 01.47 +06 11 07.33	S35	2007-12-7	2454441	14	4.1
ome Vir	11 38 27.61 +08 08 03.47	S28	2007-3-14	2454173	21	7.0
ome Vir	11 38 27.61 +08 08 03.47	S38	2008-3-9	2454534	29	16.5
nu Vir	11 45 51.56 +06 31 45.74	S28	2007-3-14	2454173	21	8.4
eps Mus	12 17 34.28 -67 57 38.65	S28	2007-2-25	2454156	26	7.2
eps Mus	12 17 34.28 -67 57 38.65	S38	2008-2-27	2454523	9	3.2
eps Mus	12 17 34.28 -67 57 38.65	S52	2009-8-1	2455044	36	12.8
gam Cru	12 31 09.96 -57 06 47.57	C35	2003-1-19	2452658	10	6.4
gam Cru	12 31 09.96 -57 06 47.57	S38	2008-2-28	2454524	28	4.4
gam Cru	12 31 09.96 -57 06 47.57	S52	2009-8-1	2455044	48	13.2
del Vir	12 55 36.21 +03 23 50.89	S08	2005-1-30	2453400	16	4.2
R Hya	13 29 42.78 -23 16 52.77	C37	2003-5-18	2452777	5	2.2
R Hya	13 29 42.78 -23 16 52.77	S38	2008-3-19	2454544	14	2.2
W Hya	13 49 02.00 -28 22 03.49	C40	2003-12-1	2452974	59	17.9
W Hya	13 49 02.00 -28 22 03.49	S38	2008-3-19	2454544	16	3.5
2 Cen	13 49 26.72 -34 27 02.79	S35	2007-11-14	2454418	18	1.8
alp Boo	14 15 39.67 +19 10 56.67	C25	2001-3-26	2451994	44	6.9
alp Boo	14 15 39.67 +19 10 56.67	C27	2001-8-29	2452150	258	40.2
alp Boo	14 15 39.67 +19 10 56.67	C34	2002-10-13	2452560	2	0.4
alp Boo	14 15 39.67 +19 10 56.67	S16	2005-12-2	2453706	7	1.1

Continued on next page

Table 4 – continued from previous page

Target	R.A. Declination (J2000)	Sequence	Epoch UTC	Epoch JD	No. of Exp.	Total Exp. Time (s)
alp Boo	14 15 39.67 +19 10 56.67	S36	2008-1-5	2454470	73	2.6
alp Boo	14 15 39.67 +19 10 56.67	S53	2009-8-29	2455072	25	2.1
alp Cen	14 39 36.49 -60 50 02.37	C40	2003-12-1	2452974	50	12.2
alp Cen	14 39 36.49 -60 50 02.37	S38	2008-3-19	2454544	15	3.4
alp Cen	14 39 36.49 -60 50 02.37	S51	2009-7-2	2455014	338	215.0
alp Cen	14 39 36.49 -60 50 02.37	S52	2009-8-1	2455044	39	12.9
alp Cen	14 39 36.49 -60 50 02.37	S72	2012-3-29	2456015	212	67.0
bet UMi	14 50 42.33 +74 09 19.81	S82	2014-2-20	2456708	45	28.6
RR UMi	14 57 35.01 +65 55 56.86	S82	2014-2-20	2456708	45	28.6
R Ser	15 50 41.74 +15 08 01.10	S78	2013-4-15	2456397	121	77.0
del Oph	16 14 20.74 -03 41 39.56	S26	2007-1-4	2454104	15	4.7
del Oph	16 14 20.74 -03 41 39.56	S53	2009-8-29	2455072	14	3.8
U Her	16 25 47.47 +18 53 32.86	S78	2013-4-15	2456397	111	70.6
30 Her	16 28 38.55 +41 52 54.04	S22	2006-7-29	2453945	33	4.2
30 Her	16 28 38.55 +41 52 54.04	S53	2009-8-29	2455072	24	2.7
alp Sco	16 29 24.46 -26 25 55.21	C33	2002-7-12	2452467	73	48.2
alp Sco	16 29 24.46 -26 25 55.21	S31	2007-7-8	2454289	470	16.9
alp Sco	16 29 24.46 -26 25 55.21	S51	2009-7-17	2455029	68	26.4
alp TrA	16 48 39.89 -69 01 39.76	S08	2005-1-30	2453400	12	2.8
alp TrA	16 48 39.89 -69 01 39.76	S52	2009-8-1	2455044	32	12.7
alp Her	17 14 38.86 +14 23 25.08	S13	2005-8-28	2453610	17	2.4
alp Her	17 14 38.86 +14 23 25.08	S53	2009-8-29	2455072	28	2.9

Continued on next page

Table 4 – continued from previous page

Target	R.A. Declination (J2000)	Sequence	Epoch UTC	Epoch JD	No. of Exp.	Total Exp. Time (s)
VX Sgr	18 08 04.05 -22 13 26.63	S51	2009-7-17	2455029	34	14.4
eta Sgr	18 17 37.64 -36 45 42.07	S22	2006-7-30	2453946	16	4.2
eta Sgr	18 17 37.64 -36 45 42.07	S51	2009-7-17	2455029	38	15.9
X Oph	18 38 21.12 +08 50 02.75	S26	2007-1-4	2454104	26	5.1
X Oph	18 38 21.12 +08 50 02.75	S60	2010-5-26	2455342	7	2.2
R Lyr	18 55 20.10 +43 56 45.93	S13	2005-8-28	2453610	24	4.5
R Lyr	18 55 20.10 +43 56 45.93	S79	2013-6-20	2456463	11	1.7
R Aql	19 06 22.25 +08 13 48.01	S60	2010-5-26	2455342	6	1.9
R Aql	19 06 22.25 +08 13 48.01	S69	2011-7-27	2455769	225	42.3
W Aql	19 15 23.35 -07 02 50.35	S26	2007-1-4	2454104	20	4.9
chi Cyg	19 50 33.92 +32 54 50.61	S22	2006-7-29	2453945	33	5.3
T Cep	21 09 31.78 +68 29 27.20	S13	2005-8-28	2453610	22	4.4
T Cep	21 09 31.78 +68 29 27.20	S78	2013-5-29	2456441	92	58.5
W Cyg	21 36 02.50 +45 22 28.53	S79	2013-6-21	2456464	98	46.3
mu Cep	21 43 30.46 +58 46 48.16	S22	2006-7-30	2453946	35	5.5
pi1 Gru	22 22 44.21 -45 56 52.61	S22	2006-7-30	2453946	28	4.4
bet Gru	22 42 40.05 -46 53 04.48	C34	2002-10-5	2452552	40	7.8
alp PsA	22 57 39.05 -29 37 20.05	C25	2001-3-28	2451996	12	7.6
alp PsA	22 57 39.05 -29 37 20.05	C34	2002-10-19	2452566	32	20.4
alp PsA	22 57 39.05 -29 37 20.05	C35	2003-1-22	2452661	13	8.3
alp PsA	22 57 39.05 -29 37 20.05	S72	2012-3-30	2456016	10	6.4
bet Peg	23 03 46.46 +28 04 58.03	S13	2005-8-28	2453610	24	4.5

Continued on next page

Table 4 – continued from previous page

Target	R.A. Declination (J2000)	Sequence	Epoch UTC	Epoch JD	No. of Exp.	Total Exp. Time (s)
R Aqr	23 43 49.46 -15 17 04.14	S22	2006-7-30	2453946	15	4.7
R Cas	23 58 24.87 +51 23 19.70	S08	2005-1-30	2453400	21	5.6